

Supplementary information

Infrared-Heated Sample Introduction System to Enhance Transport Efficiency for Yeast Cell Analysis by Single Cell Inductively Coupled Plasma Mass Spectrometry

By Zichao Zhou, Mirah J. Burgener, John Burgener, and Diane Beauchemin

Table S1. Se isotopes and Ar-based polyatomic interferences¹

Isotope	Natural Abundance (%)	Interferences
⁷⁴ Se	0.87	³⁶ Ar ³⁸ Ar ⁺ , ³⁸ Ar ³⁶ S ⁺ , ⁴⁰ Ar ³⁴ S ⁺
⁷⁶ Se	9.02	³⁸ Ar ³⁸ Ar ⁺
⁷⁷ Se	7.58	⁴⁰ Ar ³⁷ Cl ⁺ , ³⁶ Ar ⁴⁰ Ar ¹ H ⁺ , ³⁸ Ar ₂ ¹ H ⁺
⁷⁸ Se	23.52	⁴⁰ Ar ³⁸ Ar ⁺ , ³⁸ Ar ⁴⁰ Ca ⁺
⁸⁰ Se	49.82	⁴⁰ Ar ₂ ⁺
⁸² Se	9.19	⁴⁰ Ar ₂ ¹ H ₂ ⁺

¹T. W. May and R. H. Wiedmeyer, *At. Spectrosc.*,1998, **19**(5), 150-155, <https://doi.org/10.46770/AS.1998.05.002>.

Table S2. Summary of sample introduction systems used for scICPMS

Sample introduction system	Sample type	TE (%)	Sample uptake rate ($\mu\text{L}/\text{min}$)	Features	Limitations	Reference
PFA-ST nebulizer + cyclonic spray chamber	Human HeLa, A549, 16HBE	0.2	320	Fe, Cu, Zn, Mn, P and S quantification in HeLa, A549, and 16HBE cells; optimized 5 ms dwell time and 2×10^5 cells mL^{-1}	Very low TE	1
MicroMist nebulizer + Scott-type spray chamber	Human A549 cells	0.5 for A549 cells; 7.5 for solution	167	Single-cell As measurement in A549; MS-MS for interference removal; direct analysis without fixation	Very low TE	2
3D*-printed polymer microconcentric nebulizer (MCN) + single-pass spray chamber with sheath gas	Chlorella algae (3.6 μm); human endothelial cells (15.4 μm)	~ 12 for NP; 0.65 for cells	750 (peristaltic pump)	higher NP TE vs. standard system; extends upper transportable diameter to ~ 25 μm ; increasing sheath gas improved cell TE	Very low TE for large mammalian cells	3
MCN + desolvator	Bacteria (<i>B. subtilis</i>)	<1	200	U* spikes confirmed as bacterial cell events; desolvation (via heating to 140 $^{\circ}\text{C}$ than cooling to 3 $^{\circ}\text{C}$) improved TE	Very low TE; desolvation increases the background noise	4
x175 nebulizer + heated single pass 8-mL spray chamber with sheath gas port in customized heater	<i>Cyclotella meneghiniana</i>	1	30 (syringe pump)	Automated online washing with switching valves and an in-line filter; high tolerance of Mg background	Very low TE; 11 min per sample	5
High efficiency cell introduction system (HECIS): demountable	HeLa, A549, and 16HBE cells	2	10 (syringe pump)	Measurement of Mn, Fe, Co, Cu, Zn, P, and S in human cancer cells and normal human epithelial cells;	Low sample flow rate and low TE	6

capillary microflow nebulizer and single-pass spray chamber wrapped with heating wire				heating to 140 °C improved TE 10-fold		
MicroMist nebulizer + conical spray chamber with impact bead	Human THP-1 monocytes; Ag NPs (50 nm)	2	4	AgNP uptake quantification; cell-to-cell heterogeneity revealed	Low sample flow rate and low TE	7
Liquid assisted droplet ejection microfluidic chip + 160 °C cartridge heater membrane desolvator	Bovine red blood cells (RBCs)	4.5	0.3-0.5 (microfluidic chip)	Monodisperse ~50 µm droplets; microfluidic chip coupled to sciCPMS	Low sample flow rate and low TE; Fe underestimated by 25% due to incomplete vaporization of droplets	8
EnyaMist nebulizer + total consumption 10-mL single-pass spray chamber	Human A2780/A2780cis ovarian cancer cells	5-25	10 (syringe pump)	Pt uptake in A2780/A2780cis; improved TE among microflow systems for mammalian cells	Low sample flow rate and low TE; 10% MeOH modifier required	9
MCN + Asperon™ spray chamber	Algae (<i>C. ovata</i> , 20–30 µm)	31 for Au NP; 30 for 2.5 µM beads	15	Commercial system; quantification of NP bio-uptake and distribution in algae; no difference between TE of NP and micro-sized beads; nebulizer gas flow has important effect on cell integrity	Low sample flow rate and low TE; large cells can lyse; MCN prone to clogging	10
glass concentric nebulizer + heated total consumption spray chamber	Metal-tagged human PBMCs, leukemia, bone marrow	30–40	—	Mass cytometry platform; ~1000 cells/s; simultaneous multi-parametric analysis	Fixed cells only	11
Spiral-helix tubing array + concentric	Human K562 bone marrow cells	42 (30 nm AuNP)	200 (syringe pump)	High sampling rate of 40,000 cells/min; AuNP uptake in K562 cells	Custom sample introduction system	12

nebulizer + mini-coaxial chamber						
HECIS	Certified Se-enriched yeast	55–69	10 (syringe pump)	Detection of Se NP; high TE for yeast; mechanical lysis of cells	Low sample flow rate; nebulizer prone to clogging	13
MicroMist high-efficiency concentric glass nebulizer + total-consumption spray chamber in a heating block	RBCs, Raji cells, A549	40 for RBC (6 μm); 74 for Raji cells (11 μm); 23 for A549 cells (20 μm)	20 (syringe pump)	81-fold TE improvement for 20- μm cells;	Low sample flow rate; nebulizer prone to clogging; univariate optimization of 2 variables	14
HECIS	Yeast (<i>S. cerevisiae</i> , ~4 μm)	75 \pm 5	10 (high pressure pump)	High TE; sheath gas prevents wall deposition; simultaneous quantification of Mg, P, Ca, Mn, Fe, Cu, Zn by ICP time-of-flight MS	Low sample flow rate; nebulizer prone to clogging; NaCl added to reduce cell adsorption	15
High sensitivity single cell system (glass MCN, sheath gas)	Bacteria (<i>Salmonella</i> , <i>E. coli</i>)	74 for Ecoli (2.1 μm); 85 for A/sureus (0.74 μm)	10 (syringe pump)	Commercially available; high TE for smaller cells	Low sample flow rate; TE not reported for bigger cells; MCN prone to clogging	16
MicroFAST single cell system	ARPE-19 cells	81 for Pt NP; 51 for cells	10 (syringe pump)	Commercially available; high cell TE; much higher sample throughput by scICPMS than by laser ablation ICPMS	Low sample flow rate; nebulizer prone to clogging	17
HECIS	Various microorganisms (2.0–6.4 μm): cyanobacteria, algae, yeast	86 for 6.4 μm cells; 100 for 2-3.0 μm cell	10 (high pressure pump)	Total consumption; inverse relationship between cell size and TE; background signals decreased by solvent evaporation; evaporation reduced cell-wall collisions and cell breakage	Low sample flow rate; nebulizer prone to clogging	18

Microdroplet generator with desolvation system	Certified Se-enriched yeast (<i>S. cerevisiae</i> , ~6 μm)	100	0.02	Total consumption; improved detection limit; 100% TE; monodisperse droplets (23–45 μm);	Extremely low cell sample uptake rate of 20 nL/min; nebulizer prone to clogging from high salt content; matrix-sensitive	19
Custom flow cell + visual contrast calibration device + fabricated nebulizer and on axis spray chamber	Human red blood cells (~7 μm)	100	5.2 (syringe pump)	Total consumption; total flow rate of 5.20 $\mu\text{L}/\text{min}$ = 0.8 $\mu\text{L}/\text{min}$ for cell suspension and 4.4 $\mu\text{L}/\text{min}$ for sheath liquid	Low sample flow rate; nebulizer prone to clogging	20

*3D= 3 dimensional

Table references

- 1 H. Wang, B. Wang, M. Wang, L. Zheng, H. Chen, Z. Chai, Y. Zhao and W. Feng, *Analyst*, 2015, 140, 523–531, <https://doi.org/10.1039/C4AN01610F>.
- 2 F. Li, D. W. Armstrong and R. S. Houk, *Anal. Chem.*, 2005, 77, 1407–1413, <https://doi.org/10.1021/ac049188l>.
- 3 G. Kajner, Á. Béltéki, M. Cseh, Z. Geretovszky, T. Ajtai, L. Barna, M. A. Deli, B. Pap, G. Maróti and G. Galbács, *Nanomaterials*, 2023, 13, <https://doi.org/10.3390/nano13233018>.
- 4 M. V. D. Au, M. Schwinn, K. Kuhlmeier, C. Büchel and B. Meermann, *Analytica Chimica Acta*, 2019, 1077, 87–94, <https://doi.org/10.1016/j.aca.2019.05.045>.
- 5 H. Wang, M. Wang, B. Wang, L. Zheng, H. Chen, Z. Chai and W. Feng, *Anal Bioanal Chem*, 2017, 409, 1415–1423, <https://doi.org/10.1007/s00216-016-0075-y>.
- 6 A. López-Serrano Oliver, S. Baumgart, W. Bremser, S. Flemig, D. Wittke, A. Grützkau, A. Luch, A. Haase and N. Jakubowski, *J. Anal. At. Spectrom.*, 2018, 33, 1256–1263, <https://doi.org/10.1039/C7JA00395A>.
- 7 S. Meyer, A. López-Serrano, H. Mitze, N. Jakubowski and T. Schwerdtle, *Metallomics*, 2018, 10, 73–76, <https://doi.org/10.1039/C7MT00285H>.

- 8 P. E. Verboket, O. Borovinskaya, N. Meyer, D. Günther and P. S. Dittrich, *Anal. Chem.*, 2014, 86, 6012–6018, <https://doi.org/10.1021/ac501149a>.
- 9 M. Corte Rodríguez, R. Álvarez-Fernández García, E. Blanco, J. Bettmer and M. Montes-Bayón, *Anal. Chem.*, 2017, 89, 11491–11497, <https://doi.org/10.1021/acs.analchem.7b02746>.
- 10 R. C. Merrifield, C. Stephan and J. R. Lead, *Environ. Sci. Technol.*, 2018, 52, 2271–2277, <https://doi.org/10.1021/acs.est.7b04968>.
- 11 K. R. Atkuri, J. C. Stevens and H. Neubert, *Drug Metabolism and Disposition*, 2015, 43, 227–233, <https://doi.org/10.1124/dmd.114.060798>.
- 12 X. Wei, X. Zhang, R. Guo, M.-L. Chen, T. Yang, Z.-R. Xu and J.-H. Wang, *Anal. Chem.*, 2019, 91, 15826–15832, <https://doi.org/10.1021/acs.analchem.9b04122>.
- 13 R. Álvarez-Fernández García, M. Corte-Rodríguez, M. Macke, K. L. LeBlanc, Z. Mester, M. Montes-Bayón and J. Bettmer, *Analyst*, 2020, 145, 1457–1465, <https://doi.org/10.1039/C9AN01565E>.
- 14 M. Nikolić, A. Lores-Padín, T. Van Acker, T. Smets, I. Goemaere, A. Ahmad, K. Braeckmans, E. Bolea-Fernandez and F. Vanhaecke, *Talanta*, 2026, 297, 128696, <https://doi.org/10.1016/j.talanta.2025.128696>.
- 15 A. S. Groombridge, S. Miyashita, S. Fujii, K. Nagasawa, T. Okahashi, M. Ohata, T. Umemura, A. Takatsu, K. Inagaki and K. Chiba, *ANAL. SCI.*, 2013, 29, 597–603, <https://doi.org/10.2116/analsci.29.597>.
- 16 B. Gomez-Gomez, M. Corte-Rodríguez, M. T. Perez-Corona, J. Bettmer, M. Montes-Bayón and Y. Madrid, *Analytica Chimica Acta*, 2020, 1128, 116–128, <https://doi.org/10.1016/j.aca.2020.06.058>.
- 17 P. Menero-Valdés, A. Lores-Padín, B. Fernández, C. D. Quarles, M. García, H. González-Iglesias and R. Pereiro, *Talanta*, 2023, 253, 123974, <https://doi.org/10.1016/j.talanta.2022.123974>.
- 18 S. Miyashita, A. S. Groombridge, S. Fujii, A. Minoda, A. Takatsu, A. Hioki, K. Chiba and K. Inagaki, *J. Anal. At. Spectrom.*, 2014, 29, 1598–1606, <https://doi.org/10.1039/C4JA00040D>.
- 19 K. Shigeta, G. Koellensperger, E. Rampler, H. Traub, L. Rottmann, U. Panne, A. Okino and N. Jakubowski, *J. Anal. At. Spectrom.*, 2013, 28, 637, <https://doi.org/10.1039/c3ja30370e>.
- 20 Y. Cao, J. Feng, L. Tang, C. Yu, G. Mo and B. Deng, *Talanta*, 2020, 206, 120174, <https://doi.org/10.1016/j.talanta.2019.120174>.

Table S3. Operating conditions used for multivariate optimization (with a central composite design) of the IR-heated sample introduction system

Experiment #	IR-heating temperature(°C)	Sample uptake rate ($\mu\text{L min}^{-1}$)	Sampling position	Nebulizer gas flow rate (L min^{-1})	^{78}Se TE (%)	^{82}Se TE (%)
1	150	5	3	0.9	7.3	6.1
2	20	15	0	1	1.2	4.1
3	85	15	0	1	16.4	17.1
4	20	25	-3	0.9	0.8	2.8
5	85	15	0	1	16.4	16.3
6	85	15	-3	1	17.8	22.6
7	85	5	0	1	19.2	27.4
8	150	25	-3	0.9	23.4	12.2
9	85	15	0	1	17.3	16.9
10	20	25	3	1.1	0.9	1.3
11	150	5	3	1.1	0.0	0.0
12	20	5	-3	1.1	28.7	24.4
13	20	5	3	0.9	0.0	4.5
14	85	25	0	1	12.5	8.5
15	85	15	0	0.9	9.5	5.1
16	85	15	0	1	17.1	15.1
17	20	5	-3	0.9	0.8	11.1
18	150	5	-3	0.9	61.5	48.7
19	150	25	-3	1.1	28.7	16.4
20	20	5	3	1.1	0.7	1.9
21	20	25	-3	1.1	1.8	6.0
22	85	15	0	1	17.0	17.4
23	150	5	-3	1.1	47.1	68.0
24	85	15	0	1.1	15.1	16.2
25	150	25	3	1.1	16.9	54.7
26	150	15	0	1	26.8	25.8
27	85	15	3	1	10.0	6.5
28	85	15	0	1	14.6	15.8
29	85	15	0	1	15.4	16.5
30	20	25	3	0.9	0.2	0.3
31	150	25	3	0.9	5.8	5.6

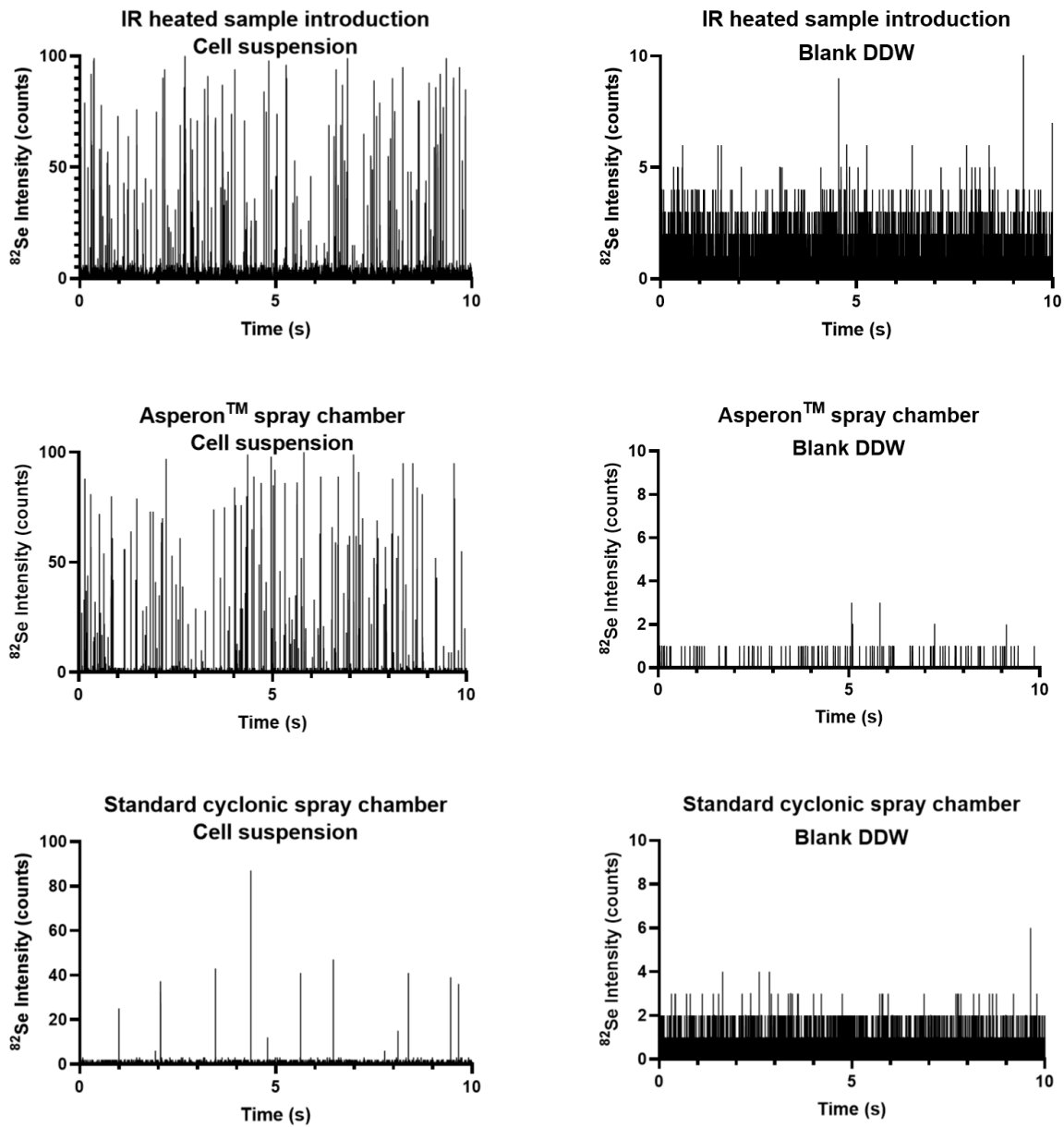


Fig. S1 Temporal profiles of a $1.96 \pm 0.20 \times 10^5$ cell suspension of SELM-1 (left) and a blank (right) with each of the 3 sample introduction systems under the conditions in Table 1.

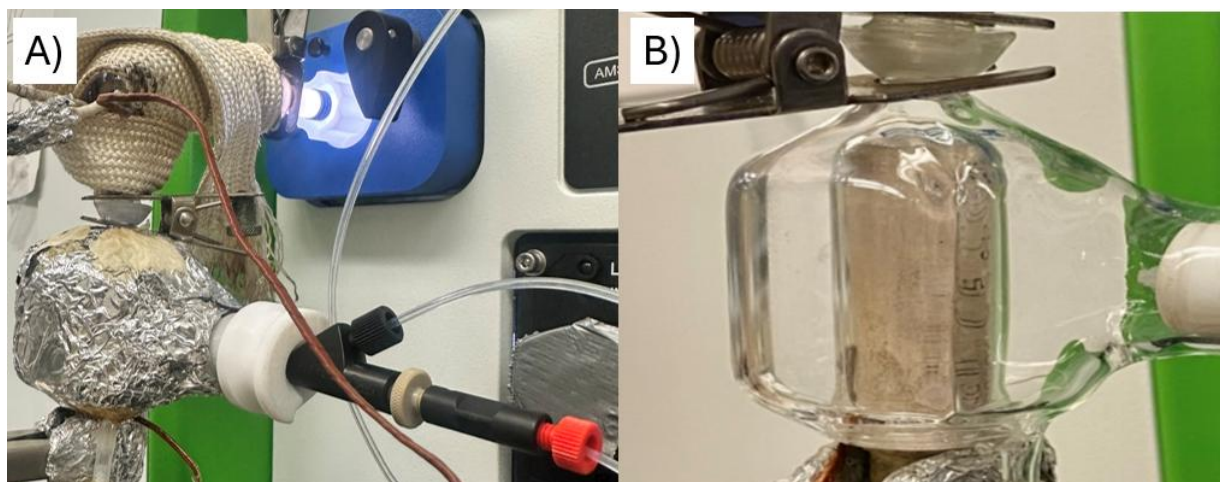


Figure S2. A) IR-heated sample introduction system, with the spray chamber wrapped with Al foil and the elbow connection to the torch wrapped with ceramic beaded IR-heater underneath insulating tape B) enlarged view of the modified 50-mL cyclonic spray chamber with IR pen heater inserted in the modified baffle

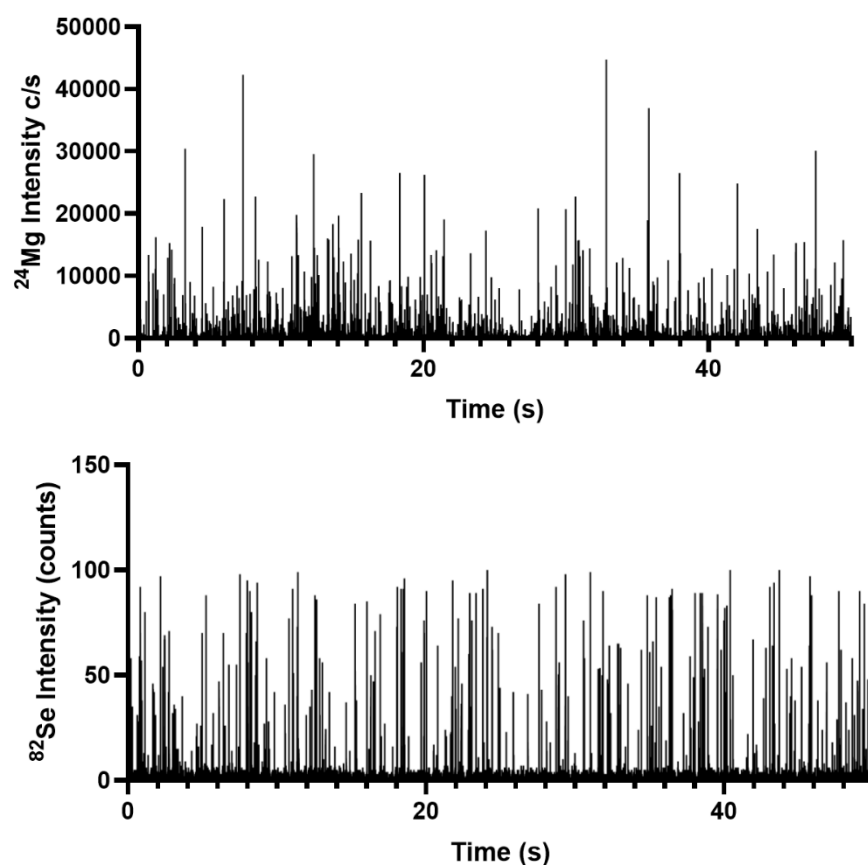
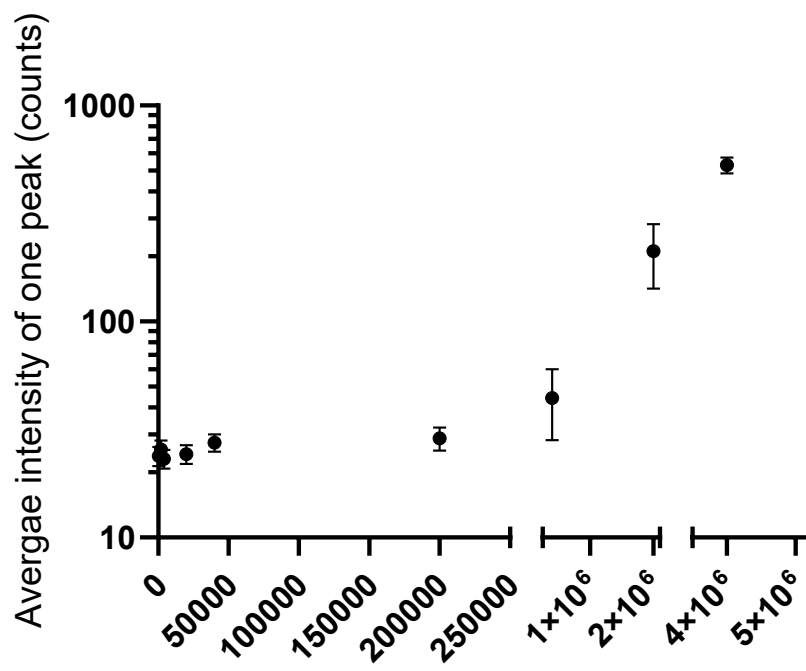
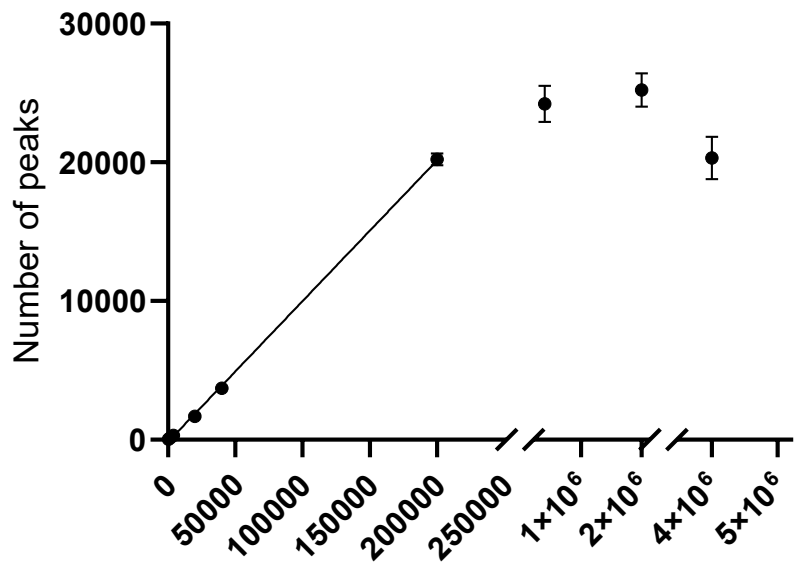


Fig. S3 ^{24}Mg and ^{82}Se temporal profiles by scICPMS from a $1.96 \pm 0.09 \times 10^5$ cells mL^{-1} SELM-1 suspension in DDW with IR-heated sample introduction system



Cell suspension number concentration (cells/mL)

Fig. S4 Number of detected cell events (top) and average intensity of cell events (bottom) for different concentrations of SELM-1 suspension (n=3)

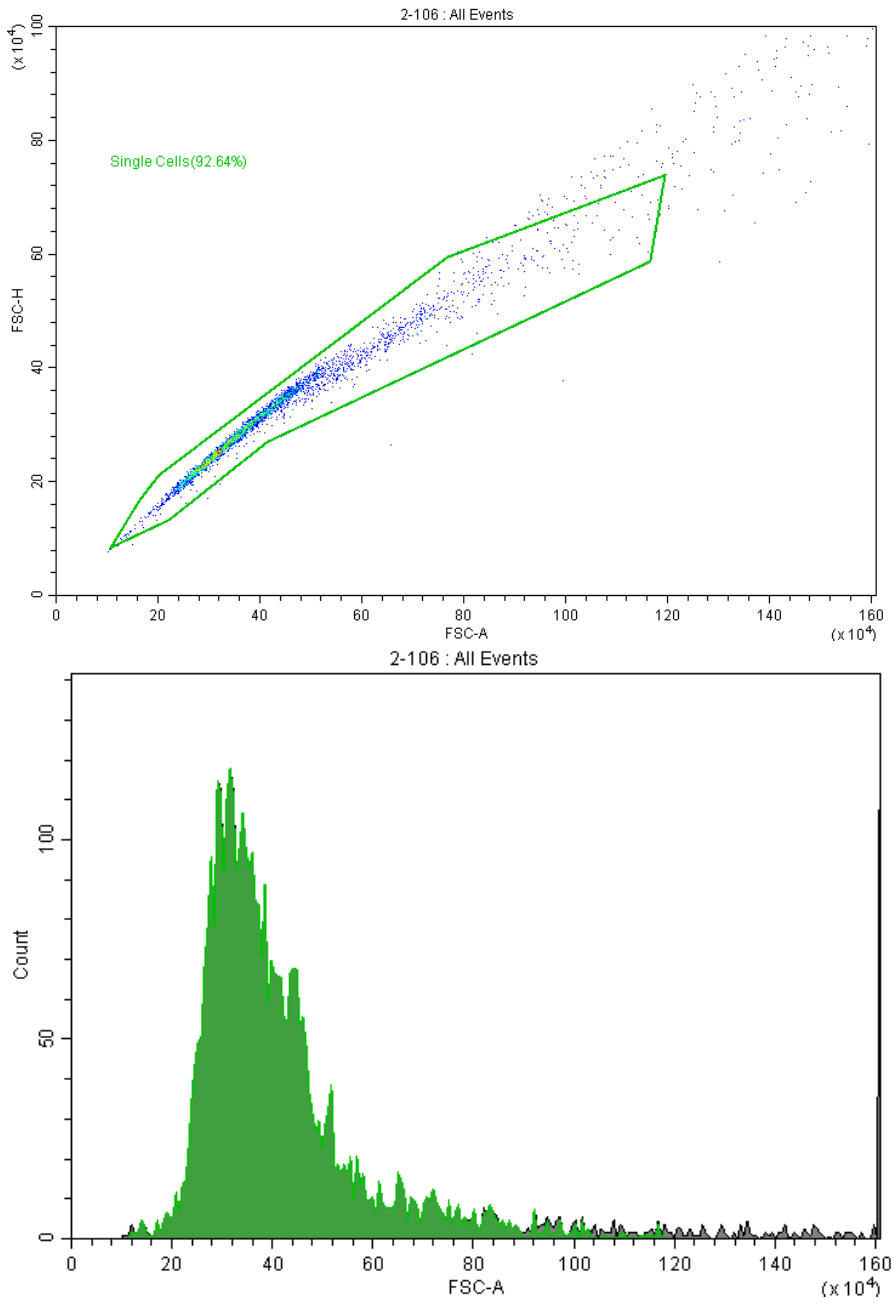


Fig. S5 Plot of flow cytometry forward scatter height (FSC-H) against forward scatter area (FSC-A) (top) and FSC-A intensity distribution (bottom) for 2×10^5 cells mL^{-1} SELM-1 in DDW

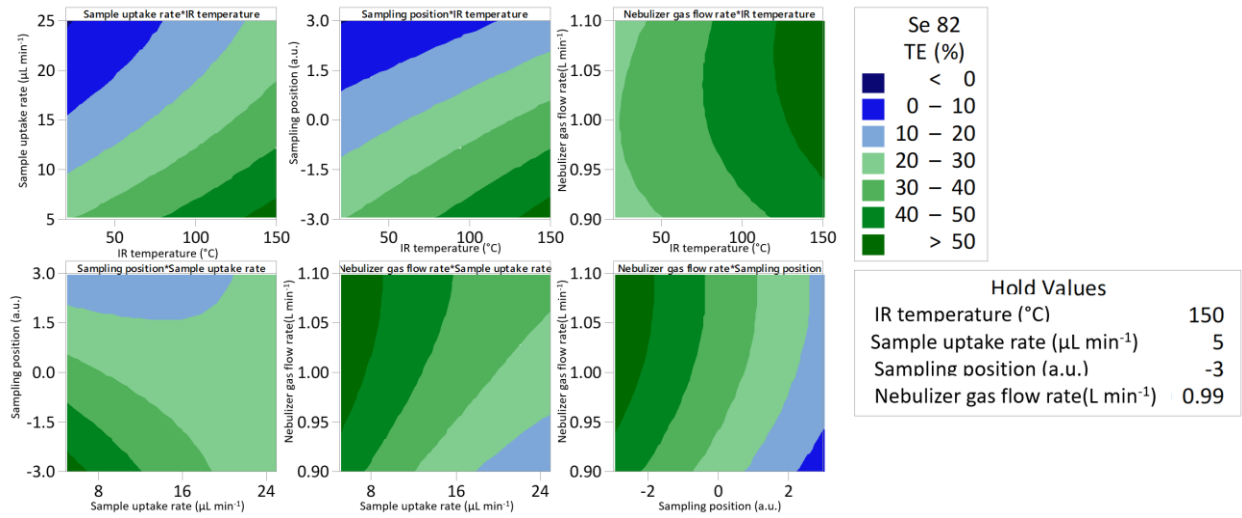


Fig. S6 Contour plots of ⁸²Se cell TE from a $1.96 \pm 0.09 \times 10^5$ cells mL⁻¹ SELM-1 suspension in DDW under different operating conditions

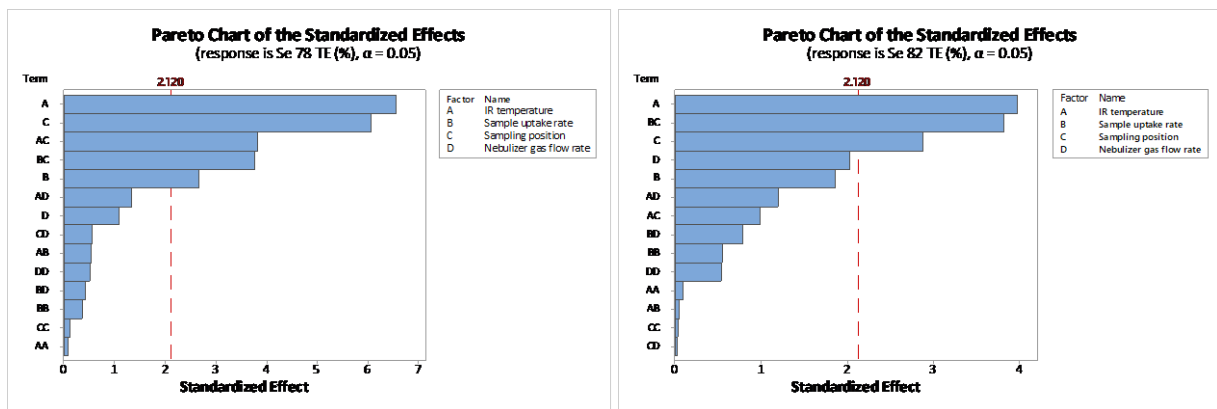


Fig. S7 (Left) Pareto chart of the standardized effect on the response of ⁷⁸Se TE (Right) Pareto chart of the standardized effect on the response of ⁸²Se TE